Indirect Detection Imprint of a CP Violating Dark Sector

Wei Chao[1]*, Michael J. Ramsey-Musolf[1,2]†, and Jiang-Hao Yu[1]‡
[1] *Amherst Center for Fundamental Interactions, Physics Department, University of Massachusetts Amherst, Amherst, MA 01003, USA, and*
[2] *Kellogg Radiation Laboratory, California Institute of Technology, Pasadena, CA 91125 USA.*

We introduce a simple scenario involving fermionic dark matter (χ) and singlet scalar mediators that may account for the Galactic Center GeV γ-ray excess while satisfying present direct detection constraints. CP-violation in the scalar potential leads to mixing between the Standard Model Higgs boson and the scalar singlet, resulting in three scalars $h_{1,2,3}$ of indefinite CP-transformation properties. This mixing enables s-wave $\chi\bar{\chi}$ annihilation into di-scalar states, followed by decays into four fermion final states. The observed γ-ray spectrum can be fitted while respecting present direct detection bounds and Higgs boson properties for $m_\chi = 60 \sim 80$ GeV, and $m_{h_3} \sim m_\chi$. Searches for the Higgs exotic decay channel $h_1 \to h_3 h_3$ at the 14 TeV LHC should be able to further probe the parameter region favored by the γ-ray excess.

arXiv:1602.05192v1 [hep-ph] 16 Feb 2016

I. INTRODUCTION

Although the presence of dark matter (DM) has been firmly established by numerous observational data *via* its gravitational effects, the particle nature of DM remains a mystery. It is imperative to search for DM in every feasible way: direct detection, indirect detection, collider searches, *etc.* Both direct detection and collider searches have observed null results, which put constraints on particle DM properties. On the other hand, indirect detection offers some hints of the particle nature of the DM. The annihilation or decays of particle DM in the galaxies are expected to produce observable fluxes of cosmic rays, such as anti-protons, positrons, gamma rays, and neutrinos. Of particular interest are gamma rays from the galactic center and the dwarf spheroidal galaxies, which are able to be detected by the Fermi Large Area Telescope (*Fermi*-LAT) [1].

Recent analyses of the *Fermi*-LAT data by several groups have identified an excess of gamma rays with several GeV energy and a nearly spherically-symmetric distribution in the center of the Milky Way, known as the Galactic Center Excess (GCE) [2–6]. Although astrophysical explanations such as millisecond pulsars have been proposed, the DM annihilation explanation of the GCE has generated much recent attention and is being widely explored. The reason is that the morphology of the GCE is consistent with what is expected from DM annihilation while complying with the observed thermal relic density.

A common and simple class of DM scenarios that can explain the GCE is the two-body DM annihilation $\chi\chi \to f\bar{f}$, where f represents a Standard Model (SM) fermion. The spectrum of the GCE has been fit well by the DM annihilation into $\bar{b}b$ with m_χ around $31 \sim 40$ GeV and the thermal averaged cross section $\langle\sigma v\rangle_{b\bar{b}} \sim \mathcal{O}(1 \sim 3) \times 10^{-26}\text{cm}^3/\text{s}$ [4, 7]. Dark matter annihilation into $\bar{\tau}\tau$ provides a acceptable fit to the spectrum with lighter m_χ around 10 GeV and smaller annihilation cross section. In these models, the DM χ interacts with the SM fermion through a mediator ϕ, which could be either scalar, fermion, or vector boson. There are two types of scenarios that explain the GCE through $2 \to 2$ annihilation : s-channel models with a neutral mediator ϕ [7], and t-channel models with a charged mediator ϕ [8, 9]. Usually in both models a heavy mediator ϕ is needed to avoid the LHC constraints, and there should be a mechanism to suppress the spin-independent DM-nucleus scattering cross section.

* Email: chao@physics.umass.edu
† Email: mjrm@physics.umass.edu
‡ Email: jhyu@physics.umass.edu

An interesting case is the fermionic DM model with a light neutral pseudo-scalar mediator [7, 10–15], in which the Lagrangian can be written as

$$\mathcal{L}_s \supset g_\chi \bar{\chi} i\gamma_5 \chi \phi + g_f \bar{f} i\gamma_5 f \phi \quad , \tag{1}$$

where χ is DM, f represents SM fermions and ϕ is a pseudo-scalar. The direct detection cross section in this case is purely spin-dependent, and thus, the direct detection rate is significantly reduced. Thus, pseudo-scalar mediated DM models have received much attention in the context of explaining the GCE, with the annihilation channels $\bar{\chi}\chi \to f\bar{f}$ [7, 10, 11]. However, there are some tensions with this model. First, the requirement of the correct relic density Ω_χ prefers a moderate value of g_f, which is constrained by collider searches [16, 17]. Second, in many ultra violet (UV) complete scenarios, ϕ is degenerate with a CP-even scalar boson, which is highly constrained by the LHC heavy Higgs searches. It is not easy to obtain a light pseudo-scalar and heavy real-scalar with large mass splitting. More importantly, the latest results on the dwarf spheroidal galaxies [20] put strong bounds on the two-body fermion final states, including $\bar{b}b$ and $\bar{\tau}\tau$ final states, creating tension between the GCE signal parameter region and the allowed dwarf spheroidal region.

The above issues might be addressed when ϕ is lighter than χ. In this case χ can annihilate into a pair of ϕ, which subsequently decay into SM particles: $\bar{\chi}\chi \to \phi\phi \to f\bar{f}f\bar{f}$ [12–15]. In this way, Ω_χ does not depend on interactions between ϕ and f, which can be quite weak. Furthermore, the DM annihilation products are four fermion final states, which is still compatible with current constraints from dwarf spheroidal galaxies. This is the so-called *hidden sector dark matter* scenario [18, 19]. In the hidden sector scenario, there are large couplings among the hidden sector particles but small couplings of the hidden particles to the SM particles. This scenario can evade the tension between tight constraints from direct detection and LHC searches and large GCE signature.

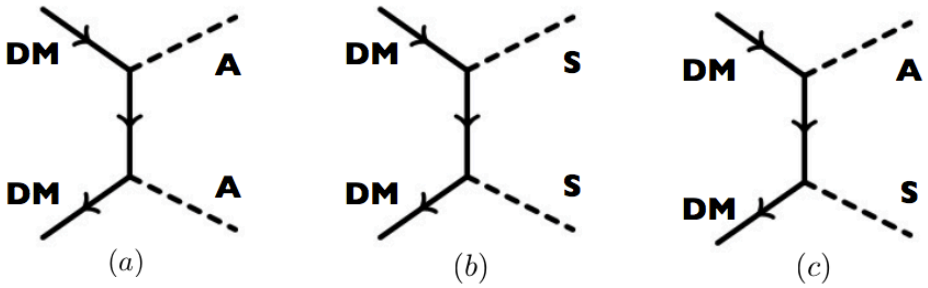

FIG. 1: The Feynman diagrams on DM annihilation to two light pseud-scalar AA (a), two light real scalar SS (b), and one light real scalar S and another light pseudo-scalar A (c).

However, there are caveats in this particular hidden sector scenario: the $\sigma(\bar{\chi}\chi \to \phi\phi)$ is typically p-wave. This gives rise to negligible indirect detection signature. Let us understand this from the parity transformation property of the initial and final states, and angular momentum conservation. We know that if the annihilation amplitude has zero orbital angular momentum, the annihilation cross section should be s-wave annihilation. Under a parity (P) transformation, the fermion-antifermion initial state transforms as $(-1)^{L+1}$, where L is the total orbital angular momentum. Depending on the final states, we have

- In Fig. 1 (a), two identical pseudo-scalars in the final state. Since the two boson final state is symmetric under interchange, the P transformation are simply $P = 1$. Therefore, although total angular momentum conservation gives rise to $L = 0, 1$, from the parity we determine that the total angular momentum is $L = 1$, which implies the anninhilation cross section is p-wave suppressed.

- In Fig. 1 (b), two identical scalars in the final state. From similar argument above, we obtain $L = 1$ and thus the anninhilation cross section is p-wave.

- In Fig. 1 (c), two different scalar bosons in the final state. In this case, there is no such exchange symmetry. Thus the orbital angular momentum could be zero. The anninhilation cross section should have s and p-waves.

From the above arguments, we note that if the final states have odd-number of pseudo-scalar, the annihilation is s-wave. Therefore, there are several ways to realize the s-wave annihilation cross section in the hidden sector DM.

- One way is that three pseudo-scalars are produced in the annihilation process, and thus the cross section $\bar{\chi}\chi \to \phi\phi\phi$ is s-wave [12]. Although phase space suppression exists, if the interactions between the DM and the pseudo-scalar are much larger than these between the DM and the SM fermions, the annihilation channel $\bar{\chi}\chi \to \phi\phi\phi$ is still larger than the s-channel $\bar{\chi}\chi \to ff$. The gamma ray signature comes from the six fermion final states. However, using this channel it is challenging to obtain both the GCE signature and the correct relic density [12]..

- Another possible way [14] is that if there are two light pseudo-scalars, the annihilation process $\bar{\chi}\chi \to \phi_1\phi_2$ is s-wave. This still needs model building efforts to split the masses of the light pseudo-scalars from the heavy real ones.

We propose a third alternative. Instead of a pseudo-scalar, a complex scalar singlet ($S = (s+ia)/\sqrt{2}$) is introduced in the hidden sector. Due to CP violation in the scalar potential, the CP-even and CP-odd field components will mix with each other and with the Standard Model Higgs boson. Thus, the resulting mass eigenstates, $h_{1,2,3}$, couple to both $\bar{\chi}\chi$ and $\bar{\chi}i\gamma_5\chi$ bilinears. Assuming $m_{h_3} \ll m_{h_2}(m_{h_1})$, which can be realized via the CP violating terms in the Higgs potential, and $m_{h_3} < m_\chi$, the process $\bar{\chi}\chi \to h_3h_3$ is thus kinematically allowed and the cross section can be s-wave. The reason is that the amplitude $\bar{\chi}\chi \to h_3h_3$ contains the parity odd bilinear $\bar{\chi}i\gamma_5\chi$. We show that this scenario can readily accommodate the GCE with thermal relic cross section, and still satisfy the other constraints. Here are the main results:

- The annihilation rate $\bar{\chi}\chi \to h_3h_3$ depends on the CP violating phases in the scalar potential. The larger the CP violating phase, the larger of the annihilation rate in the indirect detection.

- Direct detection depends on both the CP violation strength and the couplings of the scalars to the SM quarks. Since the hidden sector has small couplings to the SM particles, direct detection constraints may be avoided even though there are large CP violating phases.

- To fit the GCE spectrum, the DM annihilation cross section favors the thermal relic rate. This could be realized via sufficient CP violation. We will show that the cascade annihilation $\bar{\chi}\chi \to \phi\phi \to ffff$ could explain GCE while still being consistent with dwarf spheroidal constraints.

- If $m_{h_3} < m_{h_1}/2$, the Higgs boson h_1 will have an exotic decay channel $h_1 \to h_3h_3$. This gives us additional probe on the CP violating phases. Depending on the self-coupling of the complex scalar, the CP violating phases could be probed at the Run 2 LHC with high luminosity.

Our discussion of this scenario is as follows. We begin with the description of the CP violating complex scalar singlet model. In Sec. 3, we discuss the DM relic density and direction in this model. In Sec. 4, we present constraints on the model from oblique parameters and Higgs measurement. In Sec. 5, we discuss the GCE arising from the cascade annihilation. In Sec. 6, We study signatures of the model at the LHC. We give concluding remarks in Sec. 7.

II. THE COMPLEX CP-VIOLATING SCALAR SINGLET MODEL

As discussed in introduction, the hidden sector includes a Dirac fermion DM χ and a complex scalar singlet $S = (s + ia)/\sqrt{2}$. The interaction between the DM and the scalar singlet can be written as

$$\mathcal{L}_{\rm DM} = \bar{\chi}\gamma^\mu\partial_\mu\chi - m_0\bar{\chi}_L\chi_R - y_\chi\bar{\chi}_L S\chi_R + \text{h.c.}. \tag{2}$$

In general, the complex scalar S also interacts with the SM Higgs boson. This complex singlet scalar singlet extended SM is referred as the complex scalar singlet model (cxSM) [21, 22]. The tree-level scalar potential can be written as

$$\begin{aligned} V_{\rm cxSM} &= -\mu_h^2 H^\dagger H + \lambda_h (H^\dagger H)^2 - \mu_s^2 S^\dagger S + \lambda_s (S^\dagger S)^2 + \lambda_{sh} S^\dagger S H^\dagger H \\ &\quad + \left[-\mu_A^2 S^2 + \lambda_B S^2 (H^\dagger H) + \lambda_C S^4 + \text{h.c.}\right], \end{aligned} \tag{3}$$

where H is the SM Higgs doublet. Here although there is a Z_2 symmetry in the tree-level scalar potential, this Z_2 symmetry is broken by the Yukawa term in the Eq. 2, and thus, there is no domain wall problem. The mass term μ_A^2 and couplings λ_B, λ_C can be treated as the spurions [23], which might trigger explicit or spontaneous CP violations. We assume there is only explicit CP violation for simplicity. To parametrize the CP-violating phases, we define the rephrasing invariants as follows:

$$\delta_1 = \text{Arg}(\lambda_B \mu_A^{2*}) \,, \qquad \delta_2 = \text{Arg}(\lambda_C \lambda_B^{2*}) \,, \tag{4}$$

whose expressions in terms of physical parameters of the model will be given at the end of this section. The SM Higgs doublet and S are written in component form as follows: $H = (G^+, v_h + \hat{h} + iG^0)^T/\sqrt{2}$, and $S \equiv (v_s + \hat{s} + i\hat{a})/\sqrt{2}$, where v and v_s are vacuum expectation values (VEVs) of H and S respectively, determined by the tadpole conditions:

$$\frac{\partial V_{\rm cxSM}}{\partial \hat{\phi}_i}|_{\hat{\phi}=(\hat{h},\hat{s},\hat{a})=0} = 0. \tag{5}$$

The scalar mass matrix in the basis $(\hat{h}, \hat{s}, \hat{a})$ is

$$\mathcal{M}^2 = \begin{pmatrix} 2\lambda_h v^2 & (2\text{Re}(\lambda_B) + \lambda_{sh}) v v_s & -2\text{Im}(\lambda_B) v v_s \\ \star & 2(2\text{Re}(\lambda_C) + \lambda_s) v_s^2 & -4\text{Im}(\lambda_C) v_s^2 \\ \star & \star & 4\text{Re}(\mu_A^2) - 8\text{Re}(\lambda_C) v_s^2 - 2\text{Re}(\lambda_B) v^2 \end{pmatrix}. \tag{6}$$

Notice that the CP-violating couplings induce the mixings between $\hat{a}$ and $(\hat{h},\ \hat{s})$. The mass matrix can be diagonalized by the 3×3 unitary transformation $U^T \mathcal{M}^2 U = \text{diag}(m_{h_1}^2, m_{h_2}^2, m_{h_3}^2)$, where U takes the standard parametrization form and can be written as

$$U = \begin{pmatrix} c_{12}c_{13} & s_{12}c_{13} & s_{13} \\ -s_{12}c_{23} - c_{12}s_{23}s_{13} & c_{12}c_{23} - s_{12}s_{23}s_{13} & s_{23}c_{13} \\ s_{12}s_{23} - c_{12}c_{23}s_{13} & -c_{12}s_{23} - s_{12}c_{23}s_{13} & c_{23}c_{13} \end{pmatrix}, \tag{7}$$

with $c_{ij} \equiv \cos\theta_{ij}$ and $s_{ij} \equiv \sin\theta_{ij}$. Then the mass eigenstates $h_i = (h_1, h_2, h_3)$ can be expressed in terms of $\hat{h}_i = (\hat{h}, \hat{s}, \hat{a})$:

$$\begin{pmatrix} h_1 \\ h_2 \\ h_3 \end{pmatrix} = U_{ij}^T \begin{pmatrix} \hat{h} \\ \hat{s} \\ \hat{a} \end{pmatrix}, \tag{8}$$

where h_1 is identified as the SM Higgs boson, and h_3 is the light mediator to the DM. Here h_2 is assumed to be very heavy to avoid possible direct detection constraints. The mixing angles θ_{13} and θ_{23} parametrize the CP violating phases $\delta_{1,2}$.

The DM mass is obtained as

$$m_\chi = m_0 + \frac{1}{\sqrt{2}} y_\chi v_s, \tag{9}$$

and its interaction with the S takes the form: $y_\chi \bar{\chi}(\hat{s} + i\gamma_5 \hat{a})\chi$. Interactions in the scalar mass eigenbasis can be parametrized as

$$\mathcal{L} \supset \left[\bar{\chi}(\lambda_{si} + \lambda_{pi} i\gamma^5)\chi + \bar{f}(g_{si} + g_{pi} i\gamma^5) f\right] h_i, \tag{10}$$

where f represents SM fermions and the coupling strengths are

$$\lambda_{si} = -i y_\chi U_{2i}/\sqrt{2}, \quad \lambda_{pi} = -i y_\chi U_{3i}/\sqrt{2}, \tag{11}$$

$$g_{si} = -i U_{1i} m_f / v, \quad g_{pi} = 0. \tag{12}$$

The Feynman rules for the scalar interactions are given in Table I. Among these, the most relevant couplings are

$$\bar{\chi}\chi h_3 : \quad (-i) y_\chi (U_{23} + U_{33} i\gamma_5)/\sqrt{2}; \quad \bar{f} f h_3 : (-i) U_{13} m_f / v; \tag{13}$$

$$\bar{\chi}\chi h_1 : \quad (-i) y_\chi (U_{21} + i U_{31}\gamma_5)/\sqrt{2}; \quad \bar{f} f h_1 : (-i) U_{12} m_f / v_h. \tag{14}$$

As the hidden scalar mediator, the light mediator h_3 only has very small coupling to SM particles. This implies a small s_{13} is favored. To have a sizable coupling $\bar{\chi}\chi h_3$, s_{23} should be moderately large, which induces a large mixing between $\hat{s}$ and $\hat{a}$. Furthermore, to avoid constraints from the high mass Higgs searches [24], the mixing angle s_{12} should be small. Finally, we need a large mass splitting between h_2 and h_3, which can be realized through the CP-violating terms in the potential.

vertex	$h_i V_\mu V_\nu$	$h_i \bar{f} f$	$h_i \bar{\chi}\chi$	$h_i \bar{\chi} i\gamma_5 \chi$
	$2i U_{1i} g_{\mu\nu} m_V^2 / v_h$	$-i U_{1i} m_f / v_h$	$-i y_\chi U_{2i}/\sqrt{2}$	$-i y_\chi U_{3i}/\sqrt{2}$

TABLE I: Couplings of the scalar bosons h_i with SM particles.

Before proceeding to study constraints on the parameter space of this model, we count scalar sector physical parameters from scalar interactions, which are m_{h_1}, m_{h_2}, m_{h_3}, v, v_s, θ_{ij}, λ_s and λ_{sh}. The mass squared parameters μ_h^2 and μ_s^2 can be determined by the tadpole conditions, while other parameters can be reconstructed as

$$\mathrm{Re}(\lambda_B) = -\frac{\lambda_{sh}}{2} + \frac{1}{2vv_s}(m_{h_1}^2 U_{11}U_{21} + m_{h_2}^2 U_{12}U_{22} + m_{h_3}^2 U_{13}U_{23}), \tag{15}$$

$$\mathrm{Im}(\lambda_B) = -\frac{1}{2vv_s}(m_{h_1}^2 U_{11}U_{31} + m_{h_2}^2 U_{12}U_{32} + m_{h_3}^2 U_{13}U_{33}), \tag{16}$$

$$\mathrm{Im}(\lambda_C) = -\frac{1}{4v_s^2}(m_{h_1}^2 U_{21}U_{31} + m_{h_2}^2 U_{22}U_{32} + m_{h_3}^2 U_{23}U_{33}, \tag{17}$$

$$\mathrm{Re}(\lambda_C) = -\frac{\lambda_s}{2} + \frac{1}{4v_s^2}(m_{h_1}^2 U_{21}^2 + m_{h_2}^2 U_{22}^2 + m_{h_3}^2 U_{23}^2), \tag{18}$$

$$\mathrm{Im}(\mu_A^2) = -\frac{1}{2}\mathrm{Im}(\lambda_B)v^2 - \mathrm{Im}(\lambda_C)v_s^2, \tag{19}$$

$$\mathrm{Re}(\mu_A^2) = -\frac{1}{2}\mathrm{Re}(\lambda_B)v^2 - 2\mathrm{Re}(\lambda_C)v_s^2 - \frac{1}{4}(m_{h_1}^2 U_{31}^2 + m_{h_2}^2 U_{32}^2 + m_{h_3}^2 U_{33}^2), \tag{20}$$

$$\lambda_h = +\frac{1}{2v^2}(m_{h_1}^2 U_{11}^2 + m_{h_2}^2 U_{12}^2 + m_{h_3}^2 U_{13}^2). \tag{21}$$

The rephasing invariants can be expressed as

$$\delta_1 = \arctan\left[\frac{\mathrm{Im}(\lambda_B)}{\mathrm{Re}(\lambda_B)}\right] - \arctan\left[\frac{\mathrm{Im}(\mu_A)}{\mathrm{Re}(\mu_A)}\right], \tag{22}$$

$$\delta_2 = \arctan\left[\frac{\mathrm{Im}(\lambda_C)}{\mathrm{Re}(\lambda_C)}\right] - 2\arctan\left[\frac{\mathrm{Im}(\lambda_B)}{\mathrm{Re}(\lambda_B)}\right]. \tag{23}$$

III. RELIC DENSITY AND DIRECT DETECTION

In the standard WIMP [25] scenario, χ thermally freezes out, leaving a significant relic abundance. In this model, χ and h_3 are assumed to be in the mass range of $10 \sim 100$ GeV. h_2 is assumed to be sufficiently heavy that its contribution to the relic density is negligible. In this parameter region, the annihilation processes are $\chi\bar{\chi} \to ff$, $\chi\bar{\chi} \to WW/ZZ$ and $\chi\bar{\chi} \to h_3 h_3$. We will calculate the thermal relic cross sections in these channels.

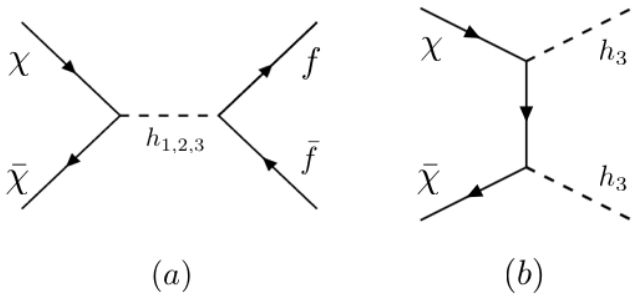

FIG. 2: Two dominant DM annihilation processes: on the left, the s-channel DM annihilation process (a), and on the right, the t-channel DM annihilation process (b).

The annihilation $\chi\bar{\chi} \to ff$ is through the s-channel h_i $(i = 1, 2, 3)$ exchange, shown in Fig. 2 (a). The s-wave part of this s-channel thermal cross section is

$$\langle \sigma v \rangle_{\bar{\chi}\chi \to \bar{f}f} \;=\; N_c \sum_{i=1,3} \frac{\lambda_{pi}^2 g_{si}^2 (m_\chi^2 - m_f^2)^{3/2}}{2\pi m_\chi [(m_{h_i}^2 - 4m_\chi^2)^2 + m_i^2 \Gamma_i^2]}, \tag{24}$$

where N_c is the number of colors for f, and Γ_i is the total decay width of h_i. Note that this thermal cross section is proportional to the coupling strengths λ_{pi} and g_{si}. We consider that new scalars couple to the DM significantly but have negligible couplings to the SM particles, which imply small couplings g_{si}. Thus we expect a small thermal cross section arising from Eq. (24), except in the presence of resonant enhancements from the s-channel mediators h_1 or h_3. When $m_\chi > m_V$, there exists the $\chi\bar{\chi} \to WW$ and $\chi\bar{\chi} \to ZZ$ channels, in which the situation is similar to that of $\chi\bar{\chi} \to f\bar{f}$. Apart from the resonance enhanced region, to obtain the correct relic density, the t-channel annihilation should be dominant over s-channel processes.

When $m_\chi > m_{h_3}$ and g_{si} is small, the dominant channel will be the t-channel process $\chi\bar{\chi} \to h_3 h_3$, shown in Fig. 2 (b). The relevant thermal cross section is

$$\begin{aligned} \langle \sigma v \rangle_{\bar{\chi}\chi \to h_3 h_3} \;=\; & \lambda_{s3}^2 \lambda_{p3}^2 \frac{m_\chi \sqrt{m_\chi^2 - m_{h_3}^2}}{2\pi (2m_\chi^2 - m_{h_3}^2)^2} + (\lambda_{s3}^4 + \lambda_{p3}^4) \frac{m_\chi^3 (m_\chi^2 - m_{h_3}^2)^{3/2}}{12\pi (2m_\chi^2 - m_{h_3}^2)^4} \langle v^2 \rangle \\ & - \lambda_{s3}^2 \lambda_{p3}^2 \frac{m_\chi^7 (32 - 52x + 20x^2 - 3x^3)}{48\pi \sqrt{m_\chi^2 - m_{h_3}^2} (2m_\chi^2 - m_{h_3}^2)^4} \langle v^2 \rangle, \end{aligned} \tag{25}$$

where $x = \frac{m_{h_3}^2}{m_\chi^2}$. The cross section only depends on the DM couplings. From Eq. 25, we notice that when there are both the scalar and pseudo-scalar interactions of h_3 with χ, the annihilation cross section could be s-wave. If the h_3 is purely scalar or pseudo-scalar, the annihilation cross section will be only p-wave. Thus the h_3 needs to be a mixture of the scalar $\hat{s}$ and pseudo-scalar $\hat{a}$, which comes from the CP-violating terms in the scalar potential.

We calculate the relic density and direct detection cross section numerically using the MicrOmegas [26], which solves the Boltzmann equations numerically and utilizes CalcHEP [27] to calculate the cross section. Mixing angles

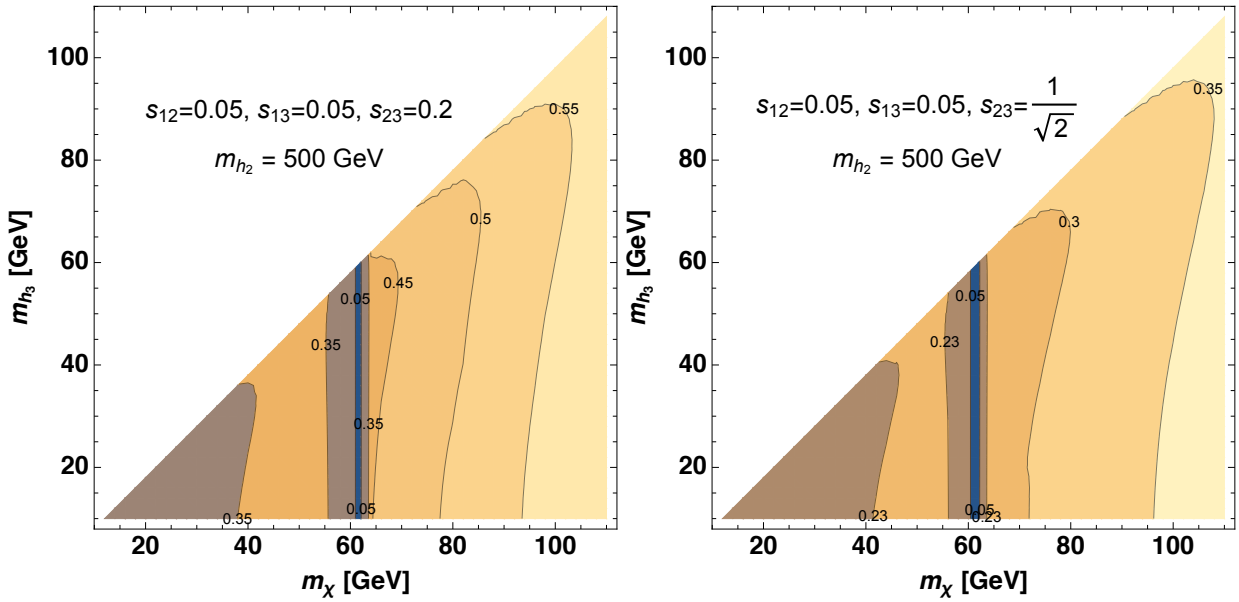

FIG. 3: Contours of the coupling strength y_χ in the (m_χ, m_{h_3}) plane, which give rise to the correct relic abundance. Mixing angles $s_{12} = s_{13} = 0.05$ and $s_{23} = 0.2$ (left panel) and $s_{23} = 1/\sqrt{2}$ (right panel) are assumed.

s_{12} and s_{13} need to be small to satisfy constraints from the Higgs measurements and electroweak precision test. On the other hand, the mixture of the $\hat{s}$ and $\hat{a}$ is parametrized by the mixing angle s_{23}, which we need to be large. When $s_{23} = 1/\sqrt{2}$ ($\theta_{23} = \pi/4$), the mixing between $\hat{s}$ and $\hat{a}$ is maximized. To illustrate, we choose two benchmark points: one with $s_{12} = s_{13} = 0.05$ and $s_{23} = 1/\sqrt{2}$, and another with $s_{12} = s_{13} = 0.05$ and $s_{23} = 0.2$. Given the mixing angles, we perform a parameter scan on $(m_\chi, m_{h_3}, y_\chi)$, and calculate the relic density for each parameter point. In Fig. 3, we show the contours of the coupling strength y_χ in the (m_χ, m_{h_3}) plane that give rise to the correct Ω_χ. We see that away from the Higgs resonance region, Ω_χ is dominated by the t-channel process. As the DM becomes heavier, the coupling y_χ needs to be larger to give rise to the correct Ω_χ. This can be seen from the $1/m_\chi^2$-dependence in the thermal cross section formulae. Near the Higgs resonance, m_χ is almost $m_{h_1}/2$. The s-channel Higgs exchange process dominates via resonant enhancement. Thus a small coupling y_χ is enough to obtain the correct relic abundance.

Given the Ω_χ-consistent parameter space, we consider the constraints from the direct detection experiments. Knowing that couplings of h_i to the SM quarks are purely scalar type, the DM−nucleus scattering only contributes to the spin-independent (SI) scattering cross section. The tightest bounds on the SI cross section come from the LUX data [28]. In this model, the SI cross section is written as

$$\sigma^{\rm SI} = \sum_{i=1,3} \frac{\mu_{\chi N}^2 U_{1i}^2 m_n^2}{\pi m_{h_i}^4 v_h^2} \left(\lambda_{si}^2 + \frac{\mu_{\chi N}^2 v^2}{2 m_\chi^2} \lambda_{pi}^2 \right) \left[Z f_p + (A - Z) f_n \right]^2 , \tag{26}$$

where $\mu_{\chi N}$ is the reduced mass, $f_{p,n}$ are the form factors of the proton and neutron, $v \sim 10^{-3}$ is the velocity of the DM. From Eq. 26, we note that although both the scalar and the pseudo-scalar interaction of the h_3 to the DM contribute to the SI cross section, the scalar interaction is dominant and the pseudo-scalar interaction exhibits velocity suppression. Fixing the coupling strength y_χ by Ω_χ, we calculate the SI cross sections for different (m_χ, m_{h_3}). Fig. 4 shows the exclusion limit on the $(m_\chi, m_{h_3}, y_\chi)$ parameter space, given the central value of the observed Ω_χ. From the Fig. 4, we see that away from the Higgs resonance region the mediator h_3 cannot be very light. This can be seen from the $1/m_{h_3}^4$-dependence in the SI cross section. Near the Higgs resonance, the coupling strength y_χ is quite small, and thus the m_{h_3} mass could be light.

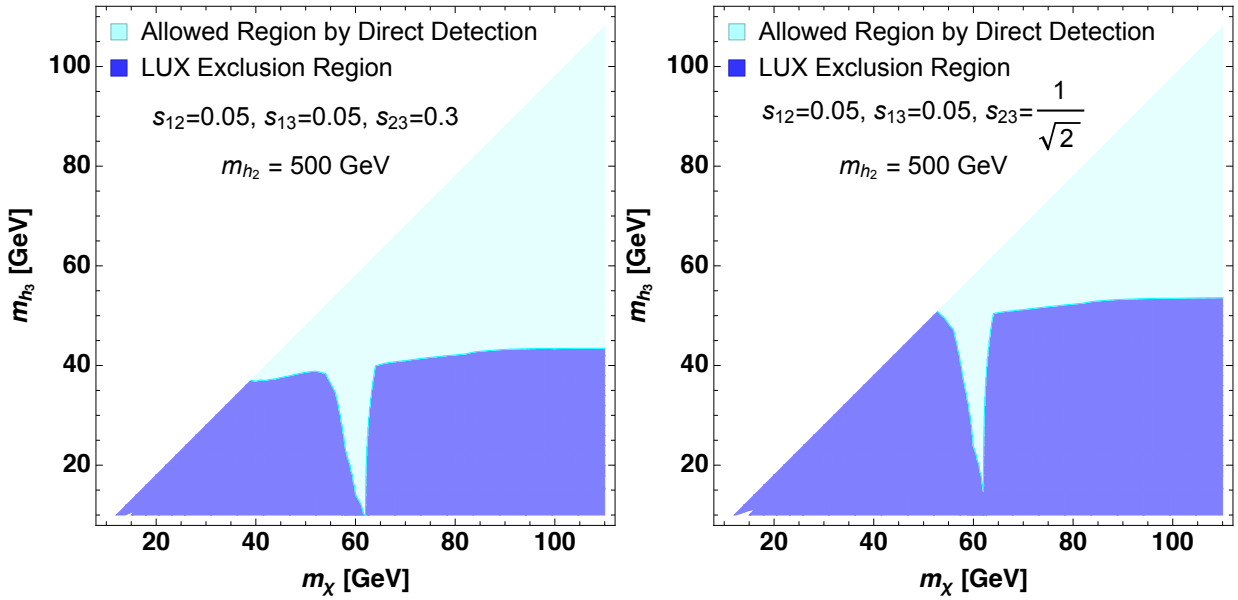

FIG. 4: Given the mixing angles $s_{12} = s_{13} = 0.05$ and $s_{23} = 0.2$ (left panel) and $s_{23} = 1/\sqrt{2}$ (right panel) and the coupling strength y_χ which give rise to the correct relic abundance, the blue region shows the parameter space excluded by the LUX data in the (m_χ, m_{h_3}) plane.

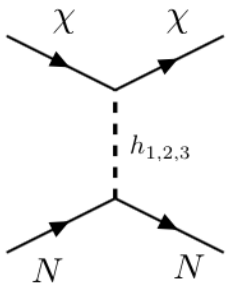

FIG. 5: DM-nucleon interaction that would generate a spin-independent direct detection signal.

IV. ELECTROWEAK PRECISION AND HIGGS CONSTRAINTS

Typically the non-observation of permanent electric dipole moments (EDMs) [29] of neutral atoms, molecules, neutron and electron place severe constraints on the strengths of CP violation. In our model, these constraints are negligible, because CP violation in the scalar potential can not lead to any pseudo-scalar type Yukawa interaction of the SM fermion, which plays a key role in generating nonzero EDMs via the two-loop Barr-Zee diagram [30]. Constraints mainly come from the LHC Higgs measurements, electroweak precision measurements and DM direct detections.

As can be seen from the Table. I, couplings of the SM-like Higgs to all SM particles are rescaled by the factor $c_{12}c_{13}$, the square of which equals to signal rates μ_{hXX} associated with Higgs measurements relative to SM Higgs expectations. In this section, we independently perform the universal Higgs fit [35] to the Higgs data from both ATLAS [31] and CMS [32, 33], where couplings of h_1 to paris of $t,\ b,\ \tau,\ W,\ Z,\ \gamma$ equal to $r_t,\ r_b,\ r_\tau,\ r_W,\ r_Z,\ r_\gamma$ in

units of the SM Higgs couplings. The χ^2 is a quadratic function of ε_i, where $\varepsilon_i \equiv r_i - 1$, and can be written as

$$\chi^2 = \sum_{i,j} (\varepsilon_i - \mu_i)(\sigma^2)^{-1}_{ij}(\varepsilon_j - \mu_j) \,, \tag{27}$$

where μ_i are the mean value of ε_i, $\sigma^2_{ij} = \sigma_i \rho_{ij} \sigma_j$ with σ_i the error of ε_i and ρ the correlation matrix. The result is shown in Fig. 6. The red solid and blue dotted lines correspond to constraints at the 68% and 95% CL respectively.

We consider the electroweak precision constraints, utilizing bounds on the oblique observables [38, 39], which are defined in terms of contributions to the vacuum polarizations of gauge bosons. The dependence of S and T parameters on the new scalars can be approximately expressed by the following one-loop terms [36]

$$\Delta S = \sum_{\kappa}^{2,3} \frac{U^2_{1\kappa}}{24\pi} \left\{ \log R_{\kappa h} + \hat{G}(M^2_\kappa, M^2_Z) - \hat{G}(m^2_h, M^2_Z) \right\} \tag{28}$$

$$\Delta T = \sum_{\kappa}^{2,3} \frac{3U^2_{1\kappa}}{16\pi s^2_W M^2_W} \left\{ M^2_Z \left[\log \frac{R_{Z\kappa}}{1 - R_{Z\kappa}} - \log \frac{R_{Zh}}{1 - R_{Zh}} \right] \right. \tag{29}$$

$$\left. - M^2_W \left[\log \frac{R_{W\kappa}}{1 - R_{W\kappa}} - \log \frac{R_{Wh}}{1 - R_{Wh}} \right] \right\} \tag{30}$$

where $c_W = \cos\theta_W$ with θ_W the weak mixing angle, $R_{\zeta\xi} \equiv M^2_\zeta / M^2_\xi$ and

$$\begin{aligned} \hat{G}(M^2_\zeta,\ M^2_\xi) \equiv & -\frac{79}{3} + 9R_{\zeta\xi} - 2R^2_{\zeta\xi} + (12 - 4R_{\zeta\xi} + R^2_{\zeta\xi})\hat{F}_{\zeta\xi} \\ & + (-10 + 18R_{\zeta\xi} - 6R^2_{\zeta\xi} + R^3_{\zeta\xi} + 9\frac{1 + R_{\zeta\xi}}{1 - R_{\zeta\xi}}) \log R_{\zeta\xi} \end{aligned} \tag{31}$$

with

$$\hat{F}_{\zeta\xi} = \begin{cases} \sqrt{R_{\zeta\xi}(R_{\zeta\xi} - 4)} \log \frac{R_{\zeta\xi} - 2 - \sqrt{R^2_{\zeta\xi} - 4R_{\zeta\xi}}}{2} & \Leftarrow R_{\zeta\xi} > 4 \\ 0 \quad \Leftarrow R_{\zeta\xi} = 4 & \\ 2\sqrt{4R_{\zeta\xi} - R^2_{\zeta\xi}} \arctan \sqrt{4R^{-1}_{\zeta\xi} - 1} & \Leftarrow R_{\zeta\xi} < 4 \end{cases} . \tag{32}$$

The most recent electroweak fit (by setting $m_{H,ref} = 126$ GeV and $m_{t,ref} = 173$ GeV) to the oblique parameters performed by the Gfitter [37] group yields

$$S = \Delta S^0 \pm \sigma_S = 0.03 \pm 0.10 \qquad T = \Delta T^0 \pm \sigma_T = 0.05 \pm 0.12 \,. \tag{33}$$

Constraints can be derived by performing $\Delta\chi^2$ fit to the data in Eq. (33), where the $\Delta\chi^2$ is given as

$$\Delta\chi^2 = \sum_{ij}^{2} (\Delta\mathcal{O}_i - \Delta\mathcal{O}^0_i)(\sigma^2_{ij})^{-1}(\Delta\mathcal{O}_j - \Delta\mathcal{O}^0_j) \,, \tag{34}$$

in which $\mathcal{O}_1 = S$, $\mathcal{O}_2 = T$ and $\sigma^2_{ij} = \sigma_i \rho_{ij} \sigma_j$ with $\rho_{11} = \rho_{22} = 1$ and $\rho_{12} = 0.891$ [37].

We show in Fig. 6 oblique parameter constraints on the mixing angles in the $\theta_{12} - \theta_{13}$ plane, by setting $m_{h_3} = 60$ GeV and $m_{h_2} = 500$ GeV. The cyan solid and black dotted lines correspond to exclusion limits at the 95% and 68% CL, respectively. It is clear that the oblique parameter constraints are much weaker than the ones from Higgs measurements. It is worth mentioning that the constraint of oblique parameters could be stronger by varying initial inputs of m_{h_2, h_3}.

As was discussed in the last section, DM direct detection experiments also constrain the size of mixing angles. By requiring the DM-nucleus scattering cross section to lie below the exclusion limit put by the LUX experiment, one gets the yellow allowed region in the $\theta_{12} - \theta_{13}$ plane in Fig. 6, where we have assumed $m_\chi \approx 70$ GeV, $m_{h_3} \approx 60$ GeV, $m_{h_2} \approx 500$ GeV and $Y_\chi \approx 0.28$ so as as to give rise to a correct relic density. The direct detection cross section is approximately proportional to to $(1 - 2\cos 2\theta_{23})$, such that there two regions allowed in Fig. 6. The reasoning of the θ_{13} being sensitive to the DM direct detection is that we set a small m_{h_3}, which is crucial for explaining the GCE.

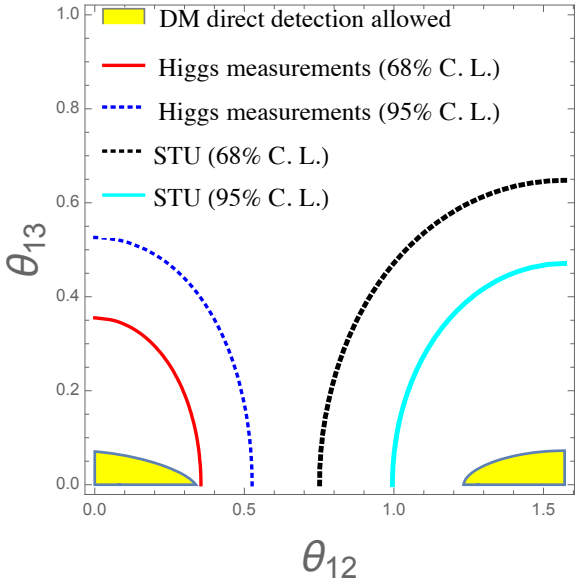

FIG. 6: Constraints on the mixing angles from the Higgs measurements, oblique parameters and the DM direct detection searches.

V. GALACTIC CENTER GEV GAMMA-RAY EXCESS

Although the direct detection and Higgs measurements put constraints on the model parameters, there still exist large parameter regions that yield indirect detection signatures. Indirect detection experiments search for the products of the DM annihilation or decay. Unlike the DM annihilation during the freeze-out, only the DM annihilation process with s-wave contribution contributes to the indirect detection signature. Off the Higgs resonance, the dominant s-wave contribution comes from the $\chi\bar{\chi} \to h_3 h_3$. To see the indirect detection signature, the $h_3 \bar{f} f$ coupling cannot be zero, and so h_3 could decay to the SM particles. Thus, CP violation is needed to have indirect detection signature. From previous sections, we learn that the h_3 has very small coupling to the SM fermion. This does not affect the annihilation cross section when the h_3 is produced on-shell because the branching ratio of h_3 does not depend on the $h_3 \bar{f} f$ coupling. Therefore, the indirect detection signatures mainly come from the cascade decay of the two on-shell h_3: the four-fermion final states via $\chi\bar{\chi} \to h_3(\to ff) h_3(\to ff)$. Among these final states, the dominant decay channel will be four-b final states, because of the relatively large bottom Yukawa coupling. This cascade annihilation and subsequent shower and hadronization produce various measurable signatures, such as gamma ray, *etc.* In the following, we will study the gamma ray spectrum of this cascade annihilation.

Consider a cascade annihilation $\chi\bar{\chi} \to \phi(\to ff)\phi(\to ff)$, where ϕ is a on-shell mediator in general. The gamma-ray spectrum can be obtained from the boost of the gamma-ray spectrum $\frac{dN_\gamma(\phi \to ff)}{dE_\gamma}$ in the ϕ rest frame. This spectrum can be easily obtained from the PYTHIA [40]. After boosting into the lab frame, the gamma-ray spectrum is written as [14]

$$\frac{dN_\gamma(\chi\bar{\chi} \to \phi\phi)}{dE_\gamma} = \frac{1}{2\beta\gamma} \int_{E_\gamma\gamma(1+\beta)}^{E_\gamma\gamma(1-\beta)} \frac{dE'_\gamma}{E'_\gamma} \frac{dN_\gamma(\phi \to ff)}{dE'_\gamma}, \tag{35}$$

where $\beta = (1 - \gamma^{-2})^{1/2}$ with the boost factor $\gamma = m_\chi / m_\phi$. Finally, we arrive at the photon flux from the DM annihilation

$$\frac{d\Phi(b,\ell)}{dE_\gamma} = \frac{\langle\sigma v\rangle_{\chi\bar{\chi}\to\phi\phi}}{2} \frac{1}{4\pi m_\chi^2} \sum_f \mathrm{Br}_{\phi\to ff} \frac{dN_\gamma(\phi \to ff)}{dE_\gamma} \int_{\mathrm{LOS}} dx \rho^2(r(b,\ell,x)), \tag{36}$$

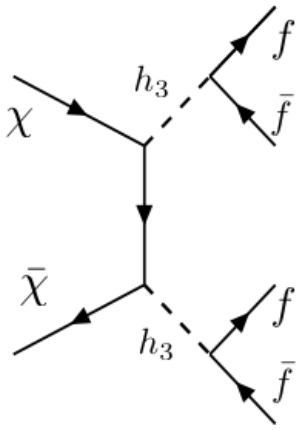

FIG. 7: DM annihilation leading to the indirect detection signatures.

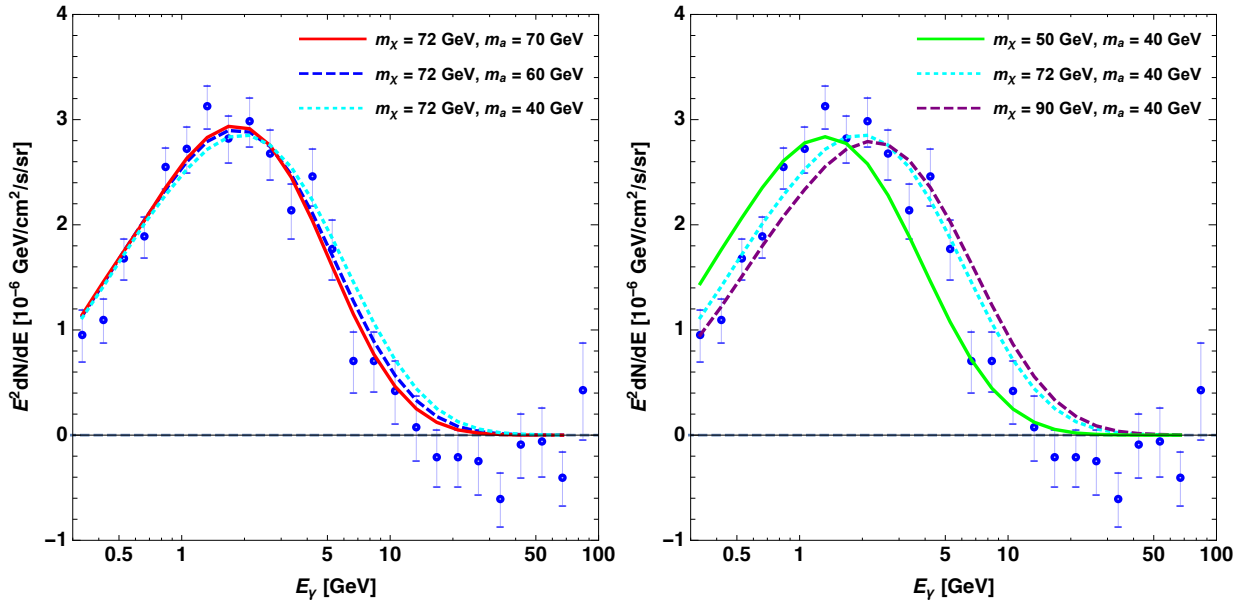
m_χ = 72 GeV, m_a = 70 GeV
m_χ = 72 GeV, m_a = 60 GeV
m_χ = 72 GeV, m_a = 40 GeV
E^2dN/dE [10^{-6} GeV/cm^2/s/sr]
E_γ [GeV]
m_χ = 50 GeV, m_a = 40 GeV
m_χ = 72 GeV, m_a = 40 GeV
m_χ = 90 GeV, m_a = 40 GeV
E^2dN/dE [10^{-6} GeV/cm^2/s/sr]
E_γ [GeV]

FIG. 8: The gamma-ray spectrum for different mediator masses with fixed DM mass (left panel) and different DM masses with fixed mediator mass (right panel). The data are taken from the spectrum of the gamma-ray excess observed in Galactic Center in Ref. [4].

where $r(b,\ell,x) = \sqrt{x^2 + R^2 - 2xR\cos\ell\cos b}$ is the distance from the Galactic center with galactic coordinates (b,ℓ), and $\rho(r)$ is the DM density profile, which is commonly taken to be the generalized NFW shape [41]. Here the J-factor is defined as $J = \int_{\rm LOS} dx \rho^2(r(b,\ell,x))$, where LOS denotes the light of sight integration. $\mathrm{Br}_{\phi\to ff}$ is the decay branching ratio of the mediator ϕ to the final state f, which is taken to be similar to the SM Higgs branching ratio.

In Fig. 8, we show the gamma-ray spectrum for different m_χ and different m_{h_3}. The spectrum shown in Fig. 8 has been normalized to corresponding to the J-factor $J = 9.09 \times 10^{23}$ GeV^2/cm^5 with $\gamma = 1.2$ in NFW profile. We find that the spectrum is very sensitive to m_χ but not to m_{h_3}. The reason is that m_χ determines the hardness of the spectrum. To obtain the favored parameter space, we define the χ^2 statistic by summing over the bins

$$\chi^2 = \sum_i \frac{(\Phi_i^{\rm data} - \Phi_i^{\rm th}(m_\chi, m_\phi, \langle\sigma v\rangle))^2}{\sigma_i^2}, \tag{37}$$

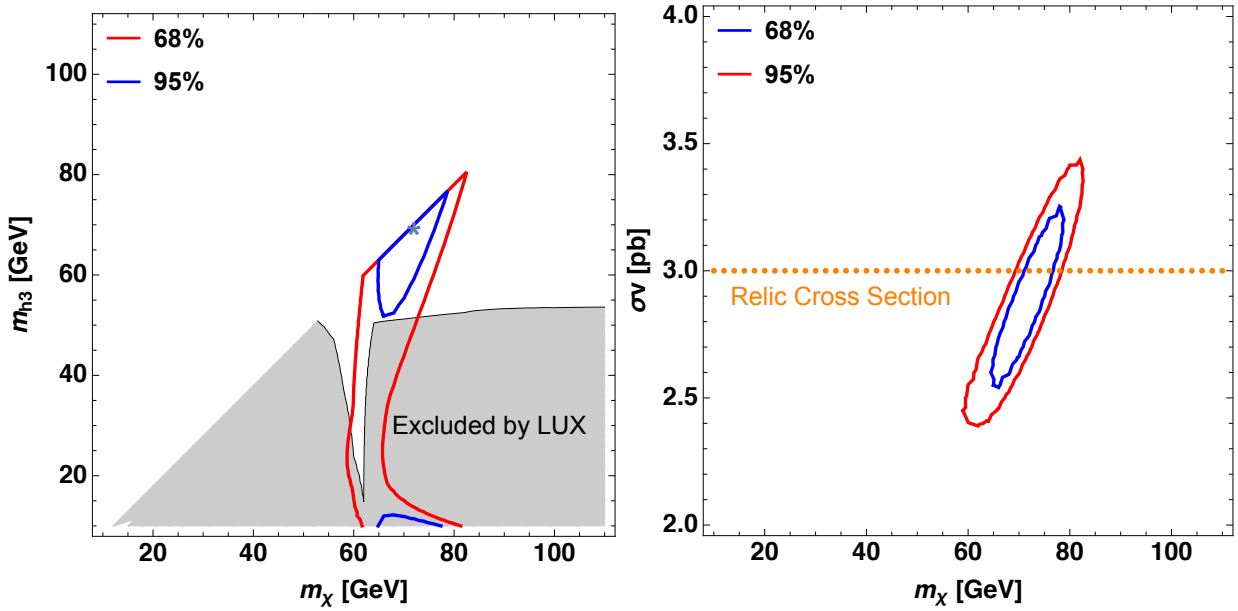

FIG. 9: On left, the favored region of the (m_χ, m_ϕ) parameter space, with $\langle\sigma v\rangle$ taken to be its best value, at 68% and 95% confidence levels. The direct detection bounds (grey region) is shown, given the benchmark parameter point: mixing angles $s_{23} = 1/\sqrt{2}$ and $s_{12} = s_{13} = 0.05$. On right panel, the favored region of the $(m_\chi, \langle\sigma v\rangle)$ parameter space, with m_ϕ taken to be its best value, at 68% and 95% confidence levels.

where $\Phi_i^{\rm data}$ and σ_i are the observed flux and the error on the data given in Ref [4]. for the bin i, and $\Phi_i^{\rm th}$ is the theoretical prediction which depends on $(m_\chi, m_\phi, \langle\sigma v\rangle)$. Then we perform a global χ^2 fit. In Fig. 9 (left panel), we show the favored region of the (m_χ, m_ϕ) parameter space at 68% and 95% CLs. For each (m_χ, m_{h_3}), the annihilation cross section is taken to be its best fit value. We also show the direct detection bounds for one of the two benchmark choices: $s_{23} = 1/\sqrt{2}$, $s_{12} = s_{13} = 0.05$. We find that to fit with the GeV gamma-ray spectrum, m_χ is preferred to be around $60 \sim 85$ GeV, which is still allowed by the tight direct detection bound. The global fit favors the degenerate mass region for m_{h_3} and m_χ with mass range $60 \sim 85$ GeV. The best fit is on the parameter point $(m_\chi, m_{h_3}) = (72, 70)$ GeV. Similarly, Fig. 9 (right panel) shows the favored region of the $(m_\chi, \langle\sigma v\rangle)$ plane at 68% and 95% CLs. For each $(m_\chi, \langle\sigma v\rangle)$, the m_{h_3} is taken to be its best fit value. We notice that the allowed annihilation cross section at 95% CL is around $2.4 \sim 3.5$ pb, which is the annihilation rate required by the correct Ω_χ. Therefore, the annihilation $\chi\bar{\chi} \to h_3 h_3$ could simultaneously explain both the GCE and Ω_χ.

The gamma-ray signature at the Galactic Center is expected to appear in other galaxies, such as, dwarf galaxies. Fermi-LAT experiments investigated the Dwarf galaxies but found a null result [20]. This puts bounds on the gamma-ray signatures from the DM annihilation, such as $b\bar{b}$, $\tau\tau$, and other channels. However, the current Fermi-LAT does not put limits on the four fermion final states with a light mediator. In principle, it is possible to re-analyse the Fermi-LAT data and obtain the limit on the four fermion final states. We leave this analysis for future study. In the following, we will comment the uncertainties on the signature and the current dwarf bounds. As shown in the Fig. 2 of Ref. [20] , if the Calore, *et. al.* data [5] are used, there is still a small parameter region which is allowed by the current dwarf bounds [42]. As was pointed out in Ref. [42], for a significantly larger integrated J-factor, which corresponds to an extreme high concentration/contraction Milky Way halo model, the signal could escape dwarf galaxy limits.

In this model, the experimental constraints implies that the hidden sector has a non-vanishing coupling to the SM sector. At the same time, the DM could have large coupling to the complex scalar. It might be possible to have self-interacting DM.

VI. HIDDEN SCALAR SEARCHES AT THE LHC

Given the favored parameter space to fit the GCE signature, we would like to know whether the LHC data are able to probe this parameter region. Collider searches provide us a complementary way to explore the GCE favored parameter space. However, in this model, due to the small coupling between the SM sector and the hidden sector, it is difficult to utilize the typical DM search channels, such as the mono-jet, mono-X plus missing energy, and other pair production of the DM final states. Fortunately, one could still investigate the Higgs exotic decays at the LHC [1]. If m_{h_3} is lighter than half of the Higgs boson mass, the Higgs boson h will decay to $h_1 \to h_3 h_3$. Similarly, if m_χ is lighter than $m_{h_1}/2$, the Higgs invisible decay channel $h_1 \to \chi\bar{\chi}$ opens. Both ATLAS and CMS looked for the Higgs invisible decay, but found null result, which puts additional constraint on the parameter space.

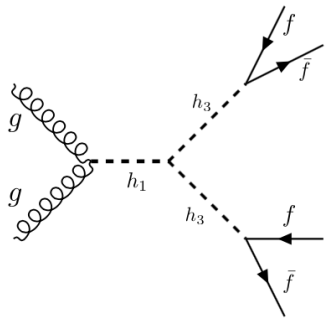

FIG. 10: Feynman diagram for the Higgs exotic decay $h_1 \to h_3 h_3 \to ffff$.

Let us investigate such Higgs exotic decay rates. Assuming $m_h > 2m_a$, the decay rate of $h_1 \to h_3 h_3$ can be written as

$$\Gamma(h_1 \to h_3 h_3) \approx \sqrt{m_h^2 - 4m_{h_3}^2}\,|\mathcal{C}|^2 /32\pi m_h^2, \tag{38}$$

where an extra factor 1/2 comes from the identical particles in the final state and the effective coupling takes the form:

$$\begin{aligned}
\mathcal{C} &= [\lambda_{sh} + 2\mathrm{Re}(\lambda_B)]\left\{v(2U_{21}U_{23}U_{13} + U_{11}U_{23}^2) + v_s(U_{21}U_{13}^2 + 2U_{11}U_{13}U_{23})\right\} \\
&+ [\lambda_{sh} - 2\mathrm{Re}(\lambda_B)]\, v(U_{11}U_{13}^2 + 2U_{31}U_{33}U_{13}) \\
&- \mathrm{Im}(\lambda_B)\left\{4v(U_{21}U_{33}U_{13} + U_{31}U_{23}U_{13} + U_{11}U_{23}U_{33}) + 2v_s(U_{31}U_{13}^2 + 2U_{11}U_{13}U_{33})\right\} \\
&+ 6v\lambda_h U_{11}U_{13}^2 + \lambda_s v_s(6U_{21}U_{23}^2 + 2U_{21}U_{33}^2 + 4U_{31}U_{33}U_{23}) \\
&+ 12\mathrm{Re}(\lambda_C)(U_{21}U_{23}^2 - U_{21}U_{33}^2 - 2U_{23}U_{31}U_{33}) \\
&+ 12\mathrm{Im}(\lambda_C)(U_{31}U_{33}^2 - U_{31}U_{23}^2 - 2U_{23}U_{21}U_{23})
\end{aligned} \tag{39}$$

In the limit of small s_{12} and s_{13}, one has

$$\Gamma(h_1 \to h_3 h_3) \approx \frac{v^2 c_{12}^2 c_{13}^4 \sqrt{m_{h_1}^2 - 4m_{h_3}^2}}{32\pi m_{h_1}^2} \left|\lambda_{sh} + 2\mathrm{Re}(\lambda_B)\cos 2\theta_{23} - 2\mathrm{Im}(\lambda_B)\sin 2\theta_{23}\right|^2 . \tag{40}$$

---

[1] At the LEP, the $e^+e^- \to Z^* \to Zh_3$ channel is highly suppressed due to the small mixing angle s_{13}. Thus there is no constraint from the LEP data

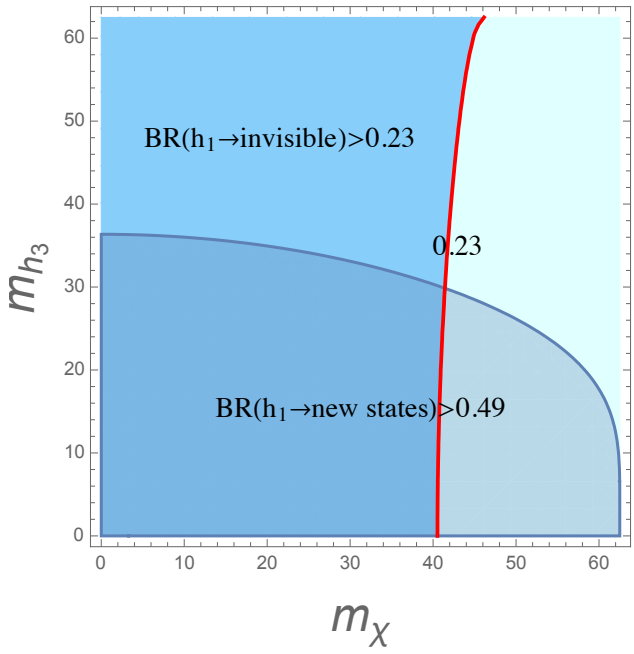

FIG. 11: Contours of constant Higgs to invisible branching ratio in the $m_\psi - m_{h_3}$ plane, setting $\theta_{12} = \theta_{13} = 0.05$, $\theta_{25} = 0.3$, $\lambda_{sh} = 0.1$, $\lambda_s = 0.01$ and $y_\chi = 0.4$. The red curve is the current upper bound on the Higgs to invisible decay branching ratio. Region surrounded by the cyan curve is excluded by the upper bound on the branching ratio of Higgs to new states.

For the case $m_{h_1} > 2m_\chi$, the Higgs to invisible decay rate can be written as

$$\Gamma(h_1 \to \bar{\chi}\chi) = \frac{(1 - c_{12}^2 c_{13}^2) Y_\chi^2}{8\pi m_{H-1}^2} (m_{h_1}^2 - 2m_\chi^2)^{3/2}. \tag{41}$$

The Higgs invisible decay has been studied at both the ATLAS and CMS [45]. The current upper limits on the Higgs invisible decay branching ratio is $\mathrm{Br}(h_1 \to \text{invisible}) < 0.23$ at the 95% CL. This limit puts constraints on the model parameters when the DM mass is lighter than the half of the Higgs boson mass. Because h_3 is lighter than χ, if the invisible decay channel opens, the new exotic decay channel $h_1 \to h_3 h_3$ will also exist. Both the invisible and new exotic channel could be classified as the undetected channel in the Higgs measurements. Assuming undetected channel, the Higgs coupling measurements put limit on the branching ratio of the Higgs boson decaying to invisible or undetected states $\mathrm{BR}(h_1 \to \text{new states})$. In Ref. [45], under the assumption $\kappa_V \leq 1$ on the Higgs boson total width, $\mathrm{BR}(h_1 \to \text{new states}) < 0.49$ at the 95% CL is obtained. We plot in Fig. 11 contours of the branching ratio of Higgs to invisible decay branching ratio in the $m_\chi - m_{h_3}$ plane by assuming $\theta_{12} = \theta_{13} = 0.05$, $\theta_{23} = 0.3$, $\lambda_{sh} = 0.1$, $\lambda_s = 0.01$ and $y_\chi = 0.4$. In Fig. 11, the red curve is the current upper bound on the Higgs to invisible decay branching ratio. Region surrounded by the cyan curve is excluded by the upper bound on the branching ratio of Higgs to new states. Parameter space outside two shaded regions satisfies the current upper limit of Higgs to invisible decays. From the Fig. 11, we learn that the Higgs invisible decay could not explore the favored GCE parameter region, which favors $m_\chi \sim 60 - 80$ GeV. On the other hand, the Higgs exotic decay branching ratio might be able to probe the GCE parameter region. In the Fig. 11, we show that when λ_s is small, the theoretical constraint $\mathrm{BR}(h \to \text{new states}) < 0.49$ is not sensitive to the GCE parameter region. In the following paragraph, we will show how the branching ratio depends on the parameter λ_s.

Except the theoretical constraints on the branching ratio of $h_1 \to h_3 h_3$, both ATLAS and CMS also studied the

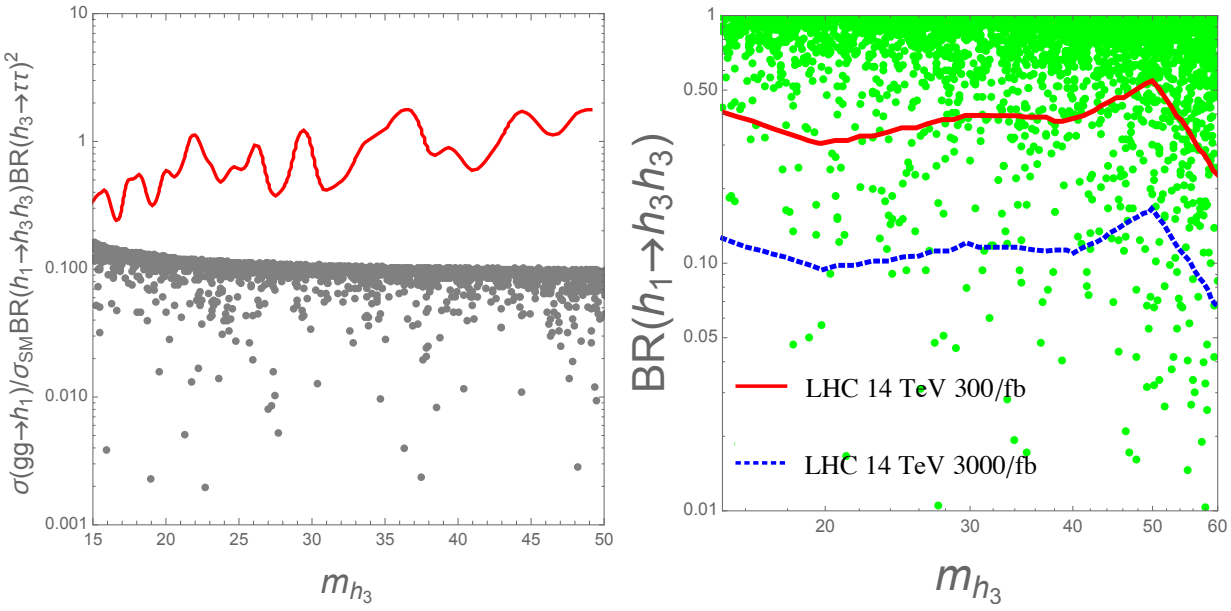

FIG. 12: Scatter plots of the signal strength as the function of m_a. On the left, the red curve is the observed limit given by the CMS collaboration [45]. On the right, the red solid curve and blue dashed curves are the theoretical projections at the 14 TeV LHC [52].

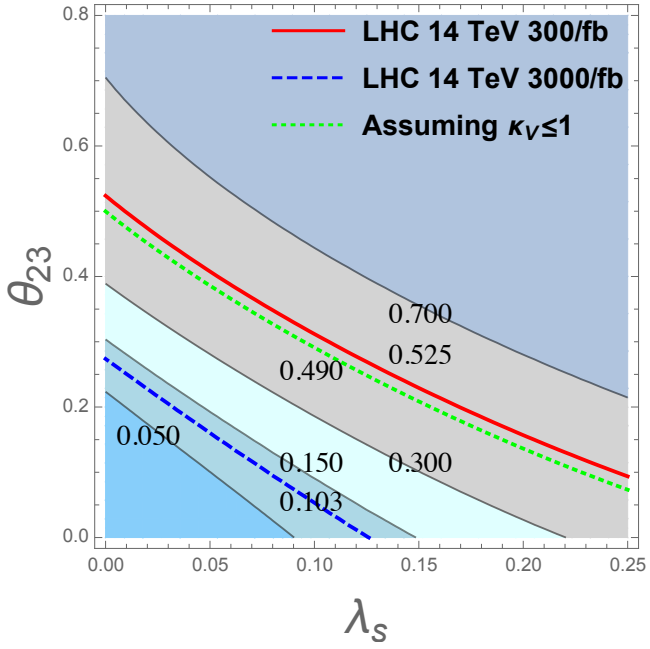

FIG. 13: Given the mixing angles $\theta_{12} = \theta_{13} = 0.05$, $\lambda_{sh} = 0.1$, and the light scalar mass $m_{h_3} = 50$ GeV, the contours of the branching ratio $\mathrm{Br}(h_1 \to h_3h_3)$ in the θ_{23} and λ_s plane are shown. The red curve and blue dashed curve are the expected limit at the 14 TeV HL-LHC with 300 fb^{-1} and 3000 fb^{-1} data [52]. The green short-dashed curve is the theoretical limit from the Ref. [45].

exotic decay channel $h_1 \to h_3h_3$ and set limits on the $\mathrm{Br}(h_1 \to h_3h_3)$. The ATLAS collaboration has searched for

a Higgs boson decaying into h_3h_3 in the $\tau\tau\mu\mu$ channel with $\sqrt{s} = 8$ TeV and the observed limit with the expected $\pm 1\sigma$ band was given in the Fig 6 of Ref. [44]. We show in Fig. 12 (left) the scatter plots of the signal strength of this model as the function of the pseudo-scalar mass, which are far below the current observed limit given by ATLAS. With higher center of mass energy and increased luminosity at the LHC Run2, we expect that better sensitivity to the parameter space can be obtained. Future LHC sensitivities have been studied in Ref. [47–52]. Ref. [52] focuses on $bb\mu\mu$ final states, and makes use of techniques of the b-tagging and the jet substructure with mass drop tagger to suppress the irreducible $bb\mu\mu$, $jj(cc)\mu\mu$, and tt backgrounds. We utilize the projected sensitivities to $\mathrm{Br}(h_1 \to h_3h_3)$ at the 14 TeV HL-LHC in Ref. [52] and recast their results to our model. Fig. 12 (right) shows the scattering plots of the signal strength of this model as the function of the light scalar mass m_{h_3}. The red-solid and green-dashed curves show that with 300 fb^{-1} and 3000 fb^{-1} data LHC could explore most of the parameter space in the model.

To explore the sensitivity of the GCE favored parameter region at the LHC Run2, we calculate the branching ratio $\mathrm{Br}(h_1 \to h_3h_3)$ in terms of the physical parameters. From the decay width in Eq. 40, we note that the decay width is quite sensitive to the two parameters θ_{23} and λ_s, but not so sensitive to λ_{sh} due to cancellation between two terms in Eq. 39. In Fig. 13, we show the contours of $\mathrm{Br}(h_1 \to h_3h_3)$ in the θ_{23} and λ_s plane, given the mixing angles $\theta_{12} = \theta_{13} = 0.05$, $\lambda_{sh} = 0.1$, and the light scalar mass $m_{h_3} = 50$ GeV. In Fig. 13, we note that as the branching ratio $\mathrm{Br}(h_1 \to h_3h_3)$ becomes smaller, smaller values of θ_{23} and λ_s are needed. Therefore, as we accumulate more data, we could probe smaller values of the parameters θ_{23} and λ_s. We know that to have s-wave DM annihilation cross section, a moderately large θ_{23} is preferred to obtain the GCE signature. With 300 fb^{-1} and 3000 fb^{-1} data we can reach the branching ratio to be as small as 0.52 and 0.10, which corresponding to θ_{23} in the region of $0.28 \sim 0.53$, which is the interesting parameter region.

VII. CONCLUSIONS

We have investigated a hidden dark matter scenario, in which the hidden sector includes a fermion DM χ and a complex scalar S. The complex scalar mixes with the SM Higgs boson with suppressed coupling. This solves the possible tension between tight constraints from direct detection and LHC searches and large indirect detection signature. To obtain large DM annihilation rate, we propose that there are the CP violations in the scalar potential. The CP violations could mix the real and pseudo-scalar parts of the complex scalar, and induce a large mass splitting for the mass eigenstates: a light h_3 and much heavier h_2. We focus on an interesting parameter region: the light scalar h_3 is lighter than the DM χ. This allows the process $\bar{\chi}\chi \to h_3h_3$ as the dominant DM annihilation channel with s-wave cross section. This annihilation channel gives rise to significant indirect detection signature and could explain the existing Galactic Center gamma-ray excess.

The relevant physical parameters are the DM and light scalar masses, the mixing angles among the Higgs boson and the real and imaginary part of the complex scalar boson: θ_{12}, θ_{13}, and θ_{23}, the Yukawa coupling between the DM and the complex scalar y_χ. To obtain the needed s-wave enhancement of DM annihilation, we requires the mixing angle between the real and imaginary part of the complex scalar boson θ_{23} to be large. On the other hand, the direct detection bounds implies small mixing angles θ_{12} and θ_{13}, and large mass splitting between h_2 and h_3. We found that the EDM constraint is negligible, but the constraints from the DM direct detection, electroweak precision and the Higgs coupling measurements are tight. Both the electroweak precision and the Higgs coupling measurements prefer small mixing angles θ_{12} and θ_{13}. These constraints force us to consider the hidden DM scenario in this model.

To explain the Galactic Center excess, the DM annihilates into the four-fermion (mainly four-b) final states *via* the cascade decay $\chi\bar{\chi} \to h_3(\to ff)h_3(\to ff)$. To fit the observed gamma-ray spectrum, the m_χ is prefered to be in the 60 to 80 GeV region. And $m_{h_3} \simeq m_\chi$ is favored. Moreover, the annihilation cross section is fitted to be in the region to have correct relic density. In short, this hidden DM model explain the gamma-ray excess. Although the dwarf

galaxies might place additional constraints, it is still possible to be compatible with the current bounds if the extreme integrated J-factor is adopted. Because the scalar h_3 cannot be too light, it is unlikely to have self-interacting DM in this hidden scalar scenario.

We also found that constraints from the Higgs invisible decay and Higgs width imply that the χ and the light scalar h_3 cannot be very light. This constraint is consistent with the observed gamma-ray signature. Although the hidden sector has small coupling to the SM Higgs boson, if h_3 is lighter than half of the Higgs mass, the $h_1 \to h_3 h_3$ is a golden channel to investigate. The 8 TeV LHC results on the exotic decay $h_1 \to h_3 h_3$ cannot probe the favored parameter region. However, we show that the future 14 TeV studies could be sensitive to the mixing angle θ_{23}, which controls the DM annihilation rate. Thus we expect that with 300 fb^{-1} and 3000 fb^{-1} data the exotic decay $h_1 \to h_3 h_3$ process will be able to probe the parameter region favored by the Galactic Center gamma-ray excess.

Acknowledgements

We thank Kevork Abazajian, Grigory Ovanesyan and Peter Winslow for helpful discussions. JHY also thank Wei Xue and Asher Berlin for useful conversation during CETUP in South Dakota. This work was supported by U.S. Department of Energy contract DE-SC0011095.

[1] M. Ackermann *et al.* [Fermi-LAT Collaboration], Phys. Rev. Lett. **108**, 011103 (2012) [arXiv:1109.0521 [astro-ph.HE]].

[2] L. Goodenough and D. Hooper, arXiv:0910.2998 [hep-ph]. D. Hooper and L. Goodenough, Phys. Lett. B **697**, 412 (2011) [arXiv:1010.2752 [hep-ph]]. D. Hooper and T. Linden, Phys. Rev. D **84**, 123005 (2011) [arXiv:1110.0006 [astro-ph.HE]].

[3] K. N. Abazajian and M. Kaplinghat, Phys. Rev. D **86**, 083511 (2012) [arXiv:1207.6047 [astro-ph.HE]]. K. N. Abazajian, N. Canac, S. Horiuchi and M. Kaplinghat, Phys. Rev. D **90**, 023526 (2014) [arXiv:1402.4090 [astro-ph.HE]].

[4] T. Daylan, D. P. Finkbeiner, D. Hooper, T. Linden, S. K. N. Portillo, N. L. Rodd and T. R. Slatyer, arXiv:1402.6703 [astro-ph.HE].

[5] F. Calore, I. Cholis and C. Weniger, JCAP **1503**, 038 (2015) doi:10.1088/1475-7516/2015/03/038 [arXiv:1409.0042 [astro-ph.CO]]. F. Calore, I. Cholis, C. McCabe and C. Weniger, Phys. Rev. D **91**, no. 6, 063003 (2015) doi:10.1103/PhysRevD.91.063003 [arXiv:1411.4647 [hep-ph]].

[6] M. Ajello *et al.* [Fermi-LAT Collaboration], arXiv:1511.02938 [astro-ph.HE].

[7] A. Berlin, D. Hooper and S. D. McDermott, Phys. Rev. D **89**, no. 11, 115022 (2014) doi:10.1103/PhysRevD.89.115022 [arXiv:1404.0022 [hep-ph]].

[8] P. Agrawal, B. Batell, D. Hooper and T. Lin, Phys. Rev. D **90**, no. 6, 063512 (2014) [arXiv:1404.1373 [hep-ph]].

[9] J. H. Yu, Phys. Rev. D **90**, no. 9, 095010 (2014) doi:10.1103/PhysRevD.90.095010 [arXiv:1409.3227 [hep-ph]].

[10] C. Boehm, M. J. Dolan, C. McCabe, M. Spannowsky and C. J. Wallace, JCAP **1405**, 009 (2014) doi:10.1088/1475-7516/2014/05/009 [arXiv:1401.6458 [hep-ph]].

[11] C. Arina, E. Del Nobile and P. Panci, Phys. Rev. Lett. **114**, 011301 (2015) doi:10.1103/PhysRevLett.114.011301 [arXiv:1406.5542 [hep-ph]].

[12] M. Abdullah, A. DiFranzo, A. Rajaraman, T. M. P. Tait, P. Tanedo and A. M. Wijangco, Phys. Rev. D **90**, 035004 (2014) doi:10.1103/PhysRevD.90.035004 [arXiv:1404.6528 [hep-ph]].

[13] A. Martin, J. Shelton and J. Unwin, Phys. Rev. D **90**, no. 10, 103513 (2014) doi:10.1103/PhysRevD.90.103513 [arXiv:1405.0272 [hep-ph]].

[14] A. Berlin, P. Gratia, D. Hooper and S. D. McDermott, Phys. Rev. D **90**, no. 1, 015032 (2014) doi:10.1103/PhysRevD.90.015032 [arXiv:1405.5204 [hep-ph]].

[15] A. Berlin, S. Gori, T. Lin and L. T. Wang, Phys. Rev. D **92**, 015005 (2015) doi:10.1103/PhysRevD.92.015005 [arXiv:1502.06000 [hep-ph]].

[16] J. Kozaczuk and T. A. W. Martin, JHEP **1504**, 046 (2015) doi:10.1007/JHEP04(2015)046 [arXiv:1501.07275 [hep-ph]].

[17] M. J. Dolan, F. Kahlhoefer, C. McCabe and K. Schmidt-Hoberg, JHEP **1503**, 171 (2015) [JHEP **1507**, 103 (2015)] doi:10.1007/JHEP07(2015)103, 10.1007/JHEP03(2015)171 [arXiv:1412.5174 [hep-ph]].

[18] J. L. Feng, H. Tu and H. B. Yu, JCAP **0810**, 043 (2008) doi:10.1088/1475-7516/2008/10/043 [arXiv:0808.2318 [hep-ph]].

[19] C. Cheung, G. Elor, L. J. Hall and P. Kumar, JHEP **1103**, 042 (2011) doi:10.1007/JHEP03(2011)042 [arXiv:1010.0022 [hep-ph]].

[20] M. Ackermann *et al.* [Fermi-LAT Collaboration], arXiv:1503.02641 [astro-ph.HE].

[21] V. Barger, P. Langacker, M. McCaskey, M. Ramsey-Musolf and G. Shaughnessy, Phys. Rev. D **79**, 015018 (2009) [arXiv:0811.0393 [hep-ph]].

[22] M. Gonderinger, H. Lim and M. J. Ramsey-Musolf, Phys. Rev. D **86**, 043511 (2012) [arXiv:1202.1316 [hep-ph]].

[23] H. E. Haber and Z. Surujon, Phys. Rev. D **86**, 075007 (2012) [arXiv:1201.1730 [hep-ph]].

[24] J. M. No and M. Ramsey-Musolf, Phys. Rev. D **89**, no. 9, 095031 (2014) [arXiv:1310.6035 [hep-ph]].

[25] G. Jungman, M. Kamionkowski and K. Griest, Phys. Rept. **267**, 195 (1996) [hep-ph/9506380].

[26] G. Belanger, F. Boudjema, A. Pukhov and A. Semenov, Comput. Phys. Commun. **176**, 367 (2007) doi:10.1016/j.cpc.2006.11.008 [hep-ph/0607059].

[27] A. Belyaev, N. D. Christensen and A. Pukhov, Comput. Phys. Commun. **184**, 1729 (2013) doi:10.1016/j.cpc.2013.01.014 [arXiv:1207.6082 [hep-ph]].

[28] D. S. Akerib *et al.* [LUX Collaboration], Phys. Rev. Lett. **112**, 091303 (2014) doi:10.1103/PhysRevLett.112.091303 [arXiv:1310.8214 [astro-ph.CO]].

[29] J. Engel, M. J. Ramsey-Musolf and U. van Kolck, Prog. Part. Nucl. Phys. **71**, 21 (2013) doi:10.1016/j.ppnp.2013.03.003 [arXiv:1303.2371 [nucl-th]].

[30] S. M. Barr and A. Zee, Phys. Rev. Lett. **65**, 21 (1990) [Phys. Rev. Lett. **65**, 2920 (1990)].

[31] The AtLAS collaboration, ATLAS-CONF-2015-044.

[32] S. Chatrchyan *et al.* [CMS Collaboration], Phys. Rev. D **89**, no. 1, 012003 (2014) doi:10.1103/PhysRevD.89.012003 [arXiv:1310.3687 [hep-ex]].

[33] S. Chatrchyan *et al.* [CMS Collaboration], Phys. Rev. D **89**, no. 9, 092007 (2014) doi:10.1103/PhysRevD.89.092007 [arXiv:1312.5353 [hep-ex]].

[34] S. Profumo, M. J. Ramsey-Musolf, C. L. Wainwright and P. Winslow, Phys. Rev. D **91**, no. 3, 035018 (2015) [arXiv:1407.5342 [hep-ph]].

[35] P. P. Giardino, K. Kannike, I. Masina, M. Raidal and A. Strumia, JHEP **1405**, 046 (2014) [arXiv:1303.3570 [hep-ph]].

[36] W. Grimus, L. Lavoura, O. M. Ogreid and P. Osland, Nucl. Phys. B **801**, 81 (2008) [arXiv:0802.4353 [hep-ph]].

[37] M. Baak *et al.*, Eur. Phys. J. C **72**, 2205 (2012) [arXiv:1209.2716 [hep-ph]].

[38] M. E. Peskin and T. Takeuchi, Phys. Rev. Lett. **65**, 964 (1990).

[39] M. E. Peskin and T. Takeuchi, Phys. Rev. D **46**, 381 (1992).

[40] T. Sjstrand *et al.*, Comput. Phys. Commun. **191**, 159 (2015) doi:10.1016/j.cpc.2015.01.024 [arXiv:1410.3012 [hep-ph]].

[41] J. F. Navarro, C. S. Frenk and S. D. M. White, Astrophys. J. **462**, 563 (1996) doi:10.1086/177173 [astro-ph/9508025].

[42] K. N. Abazajian and R. E. Keeley, arXiv:1510.06424 [hep-ph].

[43] K. A. Olive *et al.* [Particle Data Group Collaboration], Chin. Phys. C **38**, 090001 (2014).

[44] G. Aad *et al.* [ATLAS Collaboration], Phys. Rev. D **92**, no. 5, 052002 (2015) [arXiv:1505.01609 [hep-ex]].

[45] G. Aad *et al.* [ATLAS Collaboration], arXiv:1509.00672 [hep-ex].

[46] G. Aad *et al.* [ATLAS Collaboration], arXiv:1507.04548 [hep-ex].

[47] M. Carena, T. Han, G. Y. Huang and C. E. M. Wagner, JHEP **0804**, 092 (2008) doi:10.1088/1126-6708/2008/04/092 [arXiv:0712.2466 [hep-ph]].

[48] S. Chang, R. Dermisek, J. F. Gunion and N. Weiner, Ann. Rev. Nucl. Part. Sci. **58**, 75 (2008) doi:10.1146/annurev.nucl.58.110707.171200 [arXiv:0801.4554 [hep-ph]].

[49] D. E. Kaplan and M. McEvoy, Phys. Lett. B **701**, 70 (2011) doi:10.1016/j.physletb.2011.05.026 [arXiv:0909.1521 [hep-ph]].

[50] J. Cao, F. Ding, C. Han, J. M. Yang and J. Zhu, JHEP **1311**, 018 (2013) doi:10.1007/JHEP11(2013)018 [arXiv:1309.4939 [hep-ph]].

[51] D. Curtin *et al.*, Phys. Rev. D **90**, no. 7, 075004 (2014) doi:10.1103/PhysRevD.90.075004 [arXiv:1312.4992 [hep-ph]].

[52] D. Curtin, R. Essig and Y. M. Zhong, JHEP **1506**, 025 (2015) doi:10.1007/JHEP06(2015)025 [arXiv:1412.4779 [hep-ph]].